

The dynamics of starvation and recovery

2 Justin D. Yeakel * †‡§, Christopher P. Kempes †‡, and Sidney Redner †¶‡

3 *School of Natural Science, University of California Merced, Merced, CA, †The Santa Fe Institute, Santa Fe, NM, ¶Department of Physics, Boston University, Boston
4 MA, ‡Contributed equally, and §To whom correspondence should be addressed: jdyeakel@gmail.com

5 Submitted to Proceedings of the National Academy of Sciences of the United States of America

6 The eco-evolutionary dynamics of species are fundamentally
7 linked to the energetic constraints of its constituent individuals.
8 Of particular importance are the tradeoffs between reproduction
9 and the dynamics of starvation and recovery in resource-limited
10 environments. To elucidate the consequences of this tradeoff,
11 we introduce a minimal nutritional state-structured model that in-
12 corporates two classes of consumer: nutritionally replete con-
13 sumers that reproduce, and undernourished, non-reproducing
14 consumers that are susceptible to mortality. As a function of the
15 transition rates between these replete and undernourished states
16 that are determined by the presence or absence of resources,
17 the consumer populations can either undergo cyclic dynamics or
18 reach a steady state. We obtain strong constraints on starvation
19 and recovery rates by deriving allometric scaling relationships
20 and find that population dynamics subject to these constraints
21 can approach the cyclic regime but are typically driven to a steady
22 state. Moreover, we find that these rates fall within a ‘refuge’ in pa-
23 rameter space, where the probability of extinction of the consumer
24 population is minimized. Thus we identify a potential mechanism
25 that may both drive and constrain the dynamics of animal pop-
26ulations. Our model provides a natural framework that predicts
27 maximum body size for mammals by determining the relative sta-
28 bility of an otherwise homogeneous population to a mutant pop-
29 ulation with altered percent body fat. For body masses $\lesssim 10^7$ g,
30 individuals with increased energetic reserves can invade resident
31 populations, and vice versa for body mass $\gtrsim 10^7$ g, thus providing
32 a principled mechanism for a within-lineage driver of Cope’s rule.

33 foraging | starvation | reproduction

34 **Significance Statement** Energetic investment in somatic mainte-
35 nance and growth vs. reproduction directly impacts the dynamics of
36 populations among species. Here, we construct a Nutritional State-
37 structured Model (NSM) to assess the population-level effects of star-
38 vation and recovery of a consumer population in a resource-limited en-
39 vironment, and use allometric scaling relationships for mammals to es-
40 tablish all timescales and rates. Our model reveals that mammalian
41 energetic rates minimize the probability of stochastic extinction, estab-
42 lishes dynamic bounds on mammalian body size while providing inde-
43 pendent theoretical support for the energy equivalence hypothesis, and
44 provides a mechanistic driver for the evolutionary trend towards larger
45 body size known as Cope’s rule.

46 Introduction

47 The behavioral ecology of all organisms is influenced by the en-
48 ergic state of individuals, which directly influences how they
49 invest reserves in uncertain environments. Such behaviors are
50 generally manifested as tradeoffs between investing in somatic
51 maintenance and growth, or allocating energy towards repro-
52 duction (1–3). The timing of these behaviors responds to se-
53 lective pressure, as the choice of the investment impacts future
54 fitness (4–6). The influence of resource limitation on an or-
55 ganism’s ability to maintain its nutritional stores may lead to
56 repeated delays or shifts in reproduction over the course of an
57 organism’s life.

58 The balance between (a) somatic growth and maintenance,
59 and (b) reproduction depends on resource availability (7). For
60 example, reindeer invest less in calves born after harsh winters
61 (when the mother’s energetic state is depleted) than in calves
62 born after moderate winters (8). Many bird species invest dif-
63 ferently in broods during periods of resource scarcity compared

64 to normal periods (9, 10), sometimes delaying or even foregoing
65 reproduction for a breeding season (1, 11, 12). Even fresh-
66 water and marine zooplankton have been observed to avoid
67 reproduction under nutritional stress (13), and those that do
68 reproduce have lower survival rates (2). Organisms may also
69 separate maintenance and growth from reproduction over space
70 and time: many salmonids, birds, and some mammals return to
71 migratory breeding grounds to reproduce after one or multiple
72 seasons in resource-rich environments where they accumulate
73 nutritional reserves (14–16).

74 Physiology also plays an important role in regulating repro-
75 ductive expenditures during periods of resource limitation. The
76 data collected thus far has shown that diverse mammals (47
77 species in 10 families) exhibit delayed implantation, whereby
78 females postpone fetal development (blastocyst implantation)
79 until nutritional reserves can be accumulated (17, 18). Many
80 other species (including humans) suffer irregular menstrual cy-
81 cling and higher abortion rates during periods of nutritional
82 stress (19, 20). In the extreme case of unicellular organisms,
83 nutrition is unavoidably linked to reproduction because the nu-
84 tritional state of the cell regulates all aspects of the cell cycle
85 (21). The existence of so many independently evolved mech-
86 anisms across such a diverse suite of organisms highlights the im-
87 portance and universality of the fundamental tradeoff between
88 somatic and reproductive investment. However the general dy-
89 namic implications of these constraints are unknown.

90 Though straightforward conceptually, incorporating the en-
91 ergic dynamics of individuals (22) into a population-level
92 framework (22, 23) presents numerous mathematical obsta-
93 cles (24). An alternative approach involves modeling the
94 macroscale relations that guide somatic versus reproductive
95 investment in a consumer-resource system. For example,
96 macroscale Lotka-Volterra models assume that the growth rate
97 of the consumer population depends on resource density, thus
98 implicitly incorporating the requirement of resource availability
99 for reproduction (25).

100 In this work, we adopt an alternative approach in which we
101 explicitly account for resource limitation and the subsequent
102 effects of starvation. Namely, only individuals with sufficient
103 energetic reserves can reproduce. Such a constraint leads to
104 reproductive time lags due to some members of the population
105 going hungry and then recovering. Additionally, we incorporate
106 the idea that reproduction is strongly constrained allometrically
107 (3), and is not generally linearly related to resource density. As
108 we shall show, these constraints influence the ensuing popula-

Reserved for Publication Footnotes

109 tion dynamics in dramatic ways.

110 111 Nutritional state-structured model (NSM)

112 We begin by defining a minimal Nutritional State-structured 158 σ , so that R^* is positive. In fact, when the resource density
113 population Model (NSM), where the consumer population is 159 $R = 0$, the rate equation for F gives exponential growth of
114 partitioned into two states: (a) an energetically replete (full) 160 F for $\lambda > \sigma$. The condition $\sigma = \lambda$ represents a transcriti-
115 state F , where the consumer reproduces at a constant rate λ 161 cal (TC) bifurcation (31) that demarcates the physical regime
116 and does not die from starvation, and (b) an energetically defi- 162 from the unphysical regime where all densities become < 0 .
117 cient (hungry) state H , where the consumer does not reproduce 163 The biological implication of the constraint $\lambda < \sigma$ has a simple
118 but dies by starvation at rate μ . The underlying resource R 164 interpretation—the rate at which a macroscopic organism loses
119 evolves by logistic growth with an intrinsic growth rate α and a 165 mass due to lack of resources is generally much faster than the
166 rate of reproduction. As we will discuss below, this inequality
167 is a natural consequence of allometric constraints (3) for organ-
168 isms within empirically observed body size ranges.

169 carrying capacity c , which we non-dimensionalize to equal one. 170 In the physical regime of $\lambda < \sigma$, the fixed point [2] may
171 Consumers transition from the full state F to the hungry state 170 either be a stable node or a limit cycle (Fig. 1). In continuous-
172 H at a rate σ —the starvation rate—and also in proportion to 171 time systems, a limit cycle arises when a pair of complex con-
173 the absence of resources ($1 - R$). Conversely, consumers re- 172 jugate eigenvalues crosses the imaginary axis to attain positive
174 cover from state H to state F at rate $\xi\rho$ and in proportion 173 real parts (32). This Hopf bifurcation is defined by $\text{Det}(\mathbf{S}) = 0$,
175 to R , where ξ converts resources to somatic growth of con- 174 with \mathbf{S} the Sylvester matrix, which is composed of the coef-
176 sumer tissue. Resources are eaten by the consumers at rate 175 ficients of the characteristic polynomial of the Jacobian ma-
177 $\rho R + \delta$, which accounts for somatic growth and maintenance 176 trix (33). As the system parameters are tuned to be within the
178 for starving consumers, respectively, and at rate β by full con- 177 stable regime but close to the Hopf bifurcation, the amplitude
179 sumers. The NSM represents a fundamental extension of the 178 of the transient but decaying cycles become large. Given that
180 idealized starving random walk model of foraging, which focuses 179 ecological systems are constantly being perturbed (34), the on-
181 on resource depletion, to include reproduction and resource re- 180 set of transient cycles, even though they decay with time in the
182 plenishment (26–28), and is a more general formulation than 181 mean-field description, can increase the extinction risk (35–37).
183 previous models incorporating starvation (29).

184 In the mean-field approximation, in which the consumers 183 of the consumers are driven to the hungry non-reproducing
185 and resources are perfectly mixed, their densities evolve accord- 184 state. Because reproduction is inhibited, there is a low steady-
186 ing to the rate equations 185 state consumer density and a high steady-state resource den-
187

$$\begin{aligned}\dot{F} &= \lambda F + \xi\rho RH - \sigma(1-R)F, \\ \dot{H} &= \sigma(1-R)F - \xi\rho RH - \mu H, \\ \dot{R} &= \alpha R(1-R) - (\rho R + \delta)H - \beta F\end{aligned}$$

188 This system of nondimensional equations follows from a set 189 source densities (Fig. 1).
190 Whereas the relation between consumer growth rate λ and
191 the starvation rate σ defines an absolute bound of biological
192 feasibility—the TC bifurcation— σ also determines the sensitiv-
193 ity of the consumer population to changes in resource density.
194 When $\sigma \gg \lambda$, the steady-state population density is small,
195 thereby increasing the risk of stochastic extinction. On the
196 other hand, as σ decreases, the system will ultimately be poised
197 either near the TC or the Hopf bifurcation (Fig. 1). If the re-
198 sults do not appear in the growth term. As discussed above,
199 the attributes of reproduction and mortality have been explic-
200 itly apportioned to the full and hungry consumers, respectively,
201 so that the growth in the total density is decoupled from the
202 resource density.

203 Equation [1] has three fixed points: two trivial fixed points
204 at $(F^*, H^*, R^*) = (0, 0, 0)$ and $(0, 0, 1)$, and one non-trivial,
205 internal fixed point at

$$\begin{aligned}F^* &= \frac{(\sigma - \lambda)\alpha\lambda\mu^2(\mu + \xi\rho)}{A(\lambda\rho B + \mu\sigma(\beta\mu + \lambda(\delta + \rho)))}, \\ H^* &= \frac{(\sigma - \lambda)\alpha\lambda^2\mu(\mu + \xi\rho)}{A(\lambda\rho B + \mu\sigma(\beta\mu + \lambda(\delta + \rho)))}, \\ R^* &= (\sigma - \lambda)\frac{\mu}{A}.\end{aligned}$$

206 where $A = (\lambda\xi\rho + \mu\sigma)$ and $B = (\beta\mu\xi + \delta\lambda\xi - \lambda\mu)$. The sta-
207 bility of this fixed point is determined by the Jacobian matrix
208 \mathbf{J} , where each matrix element $J_{ij} = \partial\dot{X}_i/\partial X_j$ when evaluated
209 at the internal fixed point, and \mathbf{X} is the vector (F, H, R) . The
210 parameters in Eq. [1] are such that the real part of the largest
211 eigenvalue of \mathbf{J} is negative, so that the system is stable with
212 respect to small perturbations from the fixed point. Because
213 this fixed point is unique, it is the global attractor for all pop-
214 ulation trajectories for any initial condition where the resource
215 and consumer densities are both nonzero.

216 From Eq. [2], an obvious constraint on the NSM is that
217 the reproduction rate λ must be less than the starvation rate

158 σ , so that R^* is positive. In fact, when the resource density
159 $R = 0$, the rate equation for F gives exponential growth of
160 F for $\lambda > \sigma$. The condition $\sigma = \lambda$ represents a transcriti-
161 cal (TC) bifurcation (31) that demarcates the physical regime
162 from the unphysical regime where all densities become < 0 .
163 The biological implication of the constraint $\lambda < \sigma$ has a simple
164 interpretation—the rate at which a macroscopic organism loses
165 mass due to lack of resources is generally much faster than the
166 rate of reproduction. As we will discuss below, this inequality
167 is a natural consequence of allometric constraints (3) for organ-
168 isms within empirically observed body size ranges.

169 carrying capacity c , which we non-dimensionalize to equal one. 170 In the physical regime of $\lambda < \sigma$, the fixed point [2] may
171 Consumers transition from the full state F to the hungry state 170 either be a stable node or a limit cycle (Fig. 1). In continuous-
172 H at a rate σ —the starvation rate—and also in proportion to 171 time systems, a limit cycle arises when a pair of complex con-
173 the absence of resources ($1 - R$). Conversely, consumers re- 172 jugate eigenvalues crosses the imaginary axis to attain positive
174 cover from state H to state F at rate $\xi\rho$ and in proportion 173 real parts (32). This Hopf bifurcation is defined by $\text{Det}(\mathbf{S}) = 0$,
175 to R , where ξ converts resources to somatic growth of con- 174 with \mathbf{S} the Sylvester matrix, which is composed of the coef-
176 sumer tissue. Resources are eaten by the consumers at rate 175 ficients of the characteristic polynomial of the Jacobian ma-
177 $\rho R + \delta$, which accounts for somatic growth and maintenance 176 trix (33). As the system parameters are tuned to be within the
178 for starving consumers, respectively, and at rate β by full con- 177 stable regime but close to the Hopf bifurcation, the amplitude
179 sumers. The NSM represents a fundamental extension of the 178 of the transient but decaying cycles become large. Given that
180 idealized starving random walk model of foraging, which focuses 179 ecological systems are constantly being perturbed (34), the on-
181 on resource depletion, to include reproduction and resource re- 180 set of transient cycles, even though they decay with time in the
182 plenishment (26–28), and is a more general formulation than 181 mean-field description, can increase the extinction risk (35–37).
183 previous models incorporating starvation (29).

184 In the mean-field approximation, in which the consumers 183 of the consumers are driven to the hungry non-reproducing
185 and resources are perfectly mixed, their densities evolve accord- 184 state. Because reproduction is inhibited, there is a low steady-
186 ing to the rate equations 185 state consumer density and a high steady-state resource den-
187

188 When the starvation rate $\sigma \gg \lambda$, a substantial fraction
189 of the consumers are driven to the hungry non-reproducing
190 state. Because reproduction is inhibited, there is a low steady-
191 state consumer density and a high steady-state resource den-
192 sity. However, if $\sigma/\lambda \rightarrow 1$ from above, the population is
193 overloaded with energetically-replete (reproducing) individuals,
194 thereby promoting oscillations between the consumer and re-
195 source densities (Fig. 1).
196 Whereas the relation between consumer growth rate λ and
197 the starvation rate σ defines an absolute bound of biological
198 feasibility—the TC bifurcation— σ also determines the sensitiv-
199 ity of the consumer population to changes in resource density.
200 When $\sigma \gg \lambda$, the steady-state population density is small,
201 thereby increasing the risk of stochastic extinction. On the
202 other hand, as σ decreases, the system will ultimately be poised
203 either near the TC or the Hopf bifurcation (Fig. 1). If the re-
204 sults do not appear in the growth term. As discussed above,
205 the attributes of reproduction and mortality have been explic-
206 itly apportioned to the full and hungry consumers, respectively,
207 so that the growth in the total density is decoupled from the
208 resource density.

209 Equation [1] has three fixed points: two trivial fixed points
210 at $(F^*, H^*, R^*) = (0, 0, 0)$ and $(0, 0, 1)$, and one non-trivial,
211 internal fixed point at

212 common constraints and average trends across large ranges in
213 body size and species diversity. Many of these relations can be
214 derived from a small set of assumptions and below we describe a
215 framework to determine the covariation of timescales and rates
216 across the range of mammals for each of the key parameters of
217 our model (cf. (38)). We are thereby able to define the regime
218 of dynamics occupied by the entire class of mammals along with
219 the key differences between the largest and smallest mammals.
220 Nearly all of the rates described in the NSM are determined
221 by consumer metabolism, which can be used to describe a vari-
222 ety of organismal features (39). The scaling relation between an
223 organism's metabolic rate B and its body mass M at reproduc-
224 tive maturity is known to scale as $B = B_0 M^\eta$ (40), where the
225 scaling exponent η is typically close to 2/3 or 3/4 for metazoans
226 (e.g., (39)), and has taxonomic shifts for unicellular species be-
227 tween $\eta \approx 1$ in eukaryotes and $\eta \approx 1.76$ in bacteria (3, 41). An

organism's metabolic rate B is proportional to the cost of tissue maintenance in the absence of growth (i.e., when the body mass is M). By definition $B = \beta/\xi$, where β is the rate at which resources are consumed for full consumers (see Eq. [1]) and where ξ is related to the conversion efficiency of resource to consumer tissue (Supporting Information).

Several efforts have shown how a partitioning of B between growth and maintenance purposes can be used to derive a general equation for both the growth trajectories and growth rates of organisms ranging from bacteria to metazoans (3, 42–45). This relation is derived from the simple balance condition

$$B_0 m^\eta = E_m \dot{m} + B_m m,$$

where E_m is the energy needed to synthesize a unit of mass, B_m is the metabolic rate to support an existing unit of mass, and m is the mass of the organism at any point in its development. This balance has the general solution (3, 46)

$$\left(\frac{m(t)}{M}\right)^{1-\eta} = 1 - \left[1 - \left(\frac{m_0}{M}\right)^{1-\eta}\right] e^{-a(1-\eta)t/M^{1-\eta}}, \quad [4]$$

where, for $\eta < 1$, $M = (B_0/B_m)^{1/(1-\eta)}$ is the asymptotic mass, $a = B_0/E_m$, and m_0 is mass at birth, itself varying allometrically as $9.7M^{0.92}$ (47). We now use this solution to define the timescale of reproduction and recovery from starvation (Fig. 2; see (48) for a detailed presentation of these timescales). The time that it takes to reach a particular mass ϵM is given by the

$$\tau(\epsilon) = \ln \left[\frac{1 - (m_0/M)^{1-\eta}}{1 - \epsilon^{1-\eta}} \right] \frac{M^{1-\eta}}{a(1-\eta)}, \quad [5]$$

where we will define values of ϵ to describe a set of rates within our model. For the time to reproduce, $t_\lambda = \tau(\epsilon_\lambda)$, where ϵ_λ is the fraction of the asymptotic mass where an organism is reproductively mature and should be close to one (typically $\epsilon_\lambda \approx 0.95$ (42)). The growth rate is then given by $\lambda = \ln(v)/t_\lambda$ where v is the number of offspring produced, and for any constant value of ϵ_λ this will scale like $\lambda \propto M^{\eta-1}$ for $M \gg m_0$ (3, 42–45).

The rate of recovery $\rho = 1/t_\rho$ requires that an organism accrues sufficient tissue to transition from the hungry to the full state. Since only certain tissues can be digested for energy (for example the brain cannot be degraded to fuel metabolism), we define the rates for starvation, death, and recovery by the timescales required to reach, or return from, specific fractions of the replete-state mass (Fig. 3; see Supporting Information, Table I for parameterizations). We define $m_\sigma = \epsilon_\sigma M$, where $\epsilon_\sigma < 1$ is the fraction of replete-state mass where reproduction ceases. This fraction will be modified if tissue composition systematically scales with adult mass. For example, making use of the observation that body fat in mammals scales with overall body size according to $M_{\text{fat}} = f_0 M^\gamma$ and assuming that once this mass is fully digested the organism starves, this would imply that $\epsilon_\sigma = 1 - f_0 M^\gamma / M$. It follows that the recovery timescale, t_ρ , is the time to go from $m = \epsilon_\sigma \epsilon_\lambda M$ to $m = \epsilon_\lambda M$ (Fig. 2). Using Eqs. [4] and [5] this timescale is given by

simply considering an adjusted starting mass of $m'_0 = \epsilon_\sigma \epsilon_\lambda M$, in which case

$$\tau_\rho = \ln \left[\frac{1 - (\epsilon_\sigma \epsilon_\lambda)^{1-\eta}}{1 - \epsilon^{1-\eta}} \right] \frac{M^{1-\eta}}{a'(1-\eta)} \quad [6]$$

where $a' = B_0/E'_m$ accounts for possible deviations in the biosynthetic energetics during recovery (see Supporting Information). It should be noted that more complicated ontogenetic models explicitly handle storage (45), whereas this feature is implicitly covered by the body fat scaling in our framework.

To determine the starvation rate, σ , we are interested in the time required for an organism to go from a mature adult that

reproduces at rate λ , to a reduced-mass hungry state where reproduction is impossible. For starving individuals we assume that an organism must meet its maintenance requirements using the digestion of existing mass as the sole energy source. This assumption implies the following simple metabolic balance

$$\dot{m} E'_m = -B_m m \quad [7]$$

$$\dot{m} = -\frac{a'}{M^{1-\eta}} m \quad [8]$$

where E'_m is the amount of energy stored in a unit of existing body mass which differs from E_m , the energy required to synthesize a unit of biomass (45). Given the replete mass, M , of an organism, the above energy balance prescribes the mass trajectory of a non-consuming organism:

$$m(t) = M e^{-a't/M^{1-\eta}}. \quad [9]$$

The time scale for starvation is given by the time it takes $m(t)$ to reach $\epsilon_\sigma M$, which gives

$$t_\sigma = -\frac{M^{1-\eta}}{a'} \ln(\epsilon_\sigma). \quad [10]$$

The starvation rate is then $\sigma = 1/t_\sigma$, which scales with replete-state mass as $1/M^{1-\eta} \ln(1 - f_0 M^\gamma / M)$. An important feature is that σ does not have a simple scaling dependence on λ (Fig. 3), which is important for the dynamics that we later discuss.

The time to death should follow a similar relation, but defined by a lower fraction of replete-state mass, $m_\mu = \epsilon_\mu M$ where $\epsilon_\mu < \epsilon_\sigma$. Suppose, for example, that an organism dies once it has digested all fat and muscle tissues, and that muscle tissue scales with body mass according to $M_{\text{musc}} = u_0 M^\zeta$. This gives $\epsilon_\mu = 1 - (f_0 M^\gamma + u_0 M^\zeta) / M$. Muscle mass has been shown to be roughly proportional to body mass (47) in mammals and thus ϵ_μ is merely ϵ_σ minus a constant. The time to death is the total time to reach $\epsilon_\mu M$ minus the time to starve, or

$$t_\mu = -\frac{M^{1-\eta}}{a'} \ln(\epsilon_\mu) - t_\sigma, \quad [11]$$

Although the rate equations [1] are general, here we focus on parameterizations for terrestrial-bound endotherms, specifically mammals, which range from a minimum of $M \approx 1\text{g}$ (the Etruscan shrew *Suncus etruscus*) to a maximum of $M \approx 10^7\text{g}$ (the late Eocene to early Miocene Indricotheriinae). Investigating other classes of organisms would simply involve altering the metabolic exponents and scalings associate with ϵ . Moreover, we emphasize that our allometric equations describe mean relationships, and do not account for the (sometimes considerable) variance associated with individual species.

Stabilizing effects of allometric constraints

As the allometric derivations of the NSM rate laws reveal, starvation and recovery rates are not independent parameters, and the biologically relevant portion of the phase space shown in Fig. 1 is constrained via covarying parameters. Given the parameters of terrestrial endotherms, we find that the starvation rate σ and the recovery rate ρ are constrained to lie within a small window of potential values (Fig. 4) for the known range of body sizes M . We thus find that the dynamics for all mammalian body sizes are confined to the steady-state regime of the NSM and that limit-cycle behavior is precluded. Incorporating uncertainty in allometric parameters (20% variation around

the mean; Fig. 4), we find that, for larger M , the distance to the TC and Hopf bifurcation decreases. These results suggest

Dynamic and energetic barriers to body size

oscillations—both stable limit cycles and transient cycles—than mammals with larger body size, though starvation and recovery rates across all values of M fall squarely in the steady state region at some distance from the Hopf bifurcation, suggesting that cyclic population dynamics should be rare, particularly in environments where resources are limiting.

It should be noted that previous studies have used allometric constraints to explain the periodicity of cyclic populations (48–50), suggesting a period $\propto M^{0.25}$. However this relation seems to hold only for some species (51), and potential drivers range from predator and/or prey lifespans to competitive dynamics (52, 53). Statistically significant support for the existence of population cycles among mammals is relatively rare though predominantly based on time series for small mammals (54). However the longer gestational times and increased difficulty in collecting adequate data precludes obtaining similar-quality information for larger organisms such that testing this particular result is not straightforward.

Extinction risk

Within our model, higher rates of starvation result in a larger flux of the population to the hungry state. In this state reproduction is absent, thus increasing the likelihood of extinction.

From the perspective of population survival, it is the rate of starvation relative to the rate of recovery that determines the long-term dynamics of the various species (Fig. 1). We therefore examine the competing effects of cyclic dynamics vs. changes in steady state density on extinction risk as a function of σ and ρ . To this end, we computed the probability of extinction, where we define extinction as a population trajectory falling below one fifth of the allometrically constrained steady state at any time between $t = 10^5$ and $t \leq 10^8$. This procedure is repeated for 50 replicates of the continuous-time system shown in Eq. 1 for an organism of $M = 100$ grams. In each replicate the initial densities are chosen to be (XF^*, XH^*, R^*) , with X a random variable that is uniformly distributed in $[0, 2]$. By allowing the rate of starvation to vary, we assessed extinction risk across a range of values for σ and ρ between ca. 10^{-7} to 10^{-3} . As expected, higher rates of extinction correlate with both high values of σ if ρ is small, and high values of ρ if σ is small. For low values of σ and high values of ρ , the increased extinction risk results from transient cycles with larger amplitudes as the system nears the Hopf bifurcation (Fig. 5). For high values of σ and low values of ρ , higher extinction risk arises because of the decrease in the steady state consumer population density (Figs. 1B, 5). This interplay creates an ‘extinction refuge’, such that for a constrained range of σ and ρ , extinction probabilities are minimized.

We find that the allometrically constrained values of σ and ρ fall squarely within the extinction refuge (Fig. 5, white point). These values are close enough to the Hopf bifurcation to avoid low steady state densities, and far enough away to avoid large-amplitude transient cycles. The fact that allometric values of σ and ρ fall within this relatively small window supports the possibility that a selective mechanism has constrained the physiological conditions that drive starvation and recovery rates within populations. Such a mechanism would select for organism physiology that generates appropriate σ and ρ values that serve to minimize extinction risk. This selection could occur via the tuning of body fat percentages, metabolic rates, and biomass maintenance efficiencies. To summarize, our finding that the allometrically-determined parameters fall within this low extinction probability region suggests that the NSM dynamics

Metabolite transport constraints are widely thought to place strict boundaries on biological scaling (39, 55, 56) and thereby lead to specific predictions on the minimum possible body size for organisms (57). Above this bound, a number of energetic and evolutionary mechanisms have been explored to assess the costs and benefits associated with larger body masses, partic-

ularly for mammals. One important such example is the *fast-ing endurance hypothesis*, which contends that larger body size, with consequent lower metabolic rates and increased ability to maintain more endogenous energetic reserves, may buffer organisms against environmental fluctuations in resource availability (58). Over evolutionary time, terrestrial mammalian lineages show a significant trend towards larger body size (known as Cope’s rule) (59–62), and it is thought that within-lineage drivers generate selection towards an optimal upper bound of roughly 10^7 grams (59), a value that is likely limited by higher extinction risk for large taxa over longer timescales (60). These trends are thought to be driven by a combination of climate change and niche availability (62); however the underpinning energetic costs and benefits of larger body sizes, and how they influence dynamics over ecological timescales, have not been explored. We argue that the NSM provides a suitable framework to explore these issues.

The NSM correctly predicts that species with smaller masses have larger steady-state population densities (Fig. 6A). Moreover, we show that the NSM provides independent theoretical support for the energy equivalence hypothesis (63, 64). The energy equivalence hypothesis argues that the total energy use, B_{tot} , of a population is constant independent of species size (e.g. (63, 64)). This hypothesis is based on observations showing that the steady state abundance, N^* , of a species is proportional to the inverse of individual metabolism (e.g. $N^* \propto M^{-3/4}/B_0$) (e.g. (63, 64)). This is usually stated as $B_{\text{tot}} = N^* B(M) = Q$ where Q is a constant, and has been shown to hold in both mammalian and vascular plant communities (63, 64). Figure 6A shows that both F^* and H^* scale like $M^{-\eta}$ over a wide range of organism sizes and Figure 6B shows that $F^* B$ is nearly constant over this same range. This result is remarkable because it illustrates that the steady state values of the NSM combined with the derived timescales naturally give rise to the energy equivalence result. Our model shows that the equivalence breaks down at the maximum observed body sizes for mammals, suggesting that this is a hard limit where deviations outside of this range are energetically suboptimal. In the framework of our model, the total metabolic rate of F and H becomes infinite at a finite mass, occurring at the same scale where the steady state resources vanish (Fig. 6). This asymptotic behavior represents an upper bound on mammalian body size and occurs at $M_{\max} = 6.5 \times 10^7$. Moreover, M_{\max} , which is entirely determined by the population-level consequences of energetic constraints, is remarkably close to the maximum body size observed in the North American mammalian fossil record (59) as well as the mass predicted from an evolutionary model of body size evolution (60).

We contend that the NSM provides a mechanistic understanding of the energetic dynamics that give rise to both observed limitations on mammalian body size as well as the observed trend towards larger body size over evolutionary time. The NSM predicts that the steady state resource density R^* decreases with increasing body size of the consumer population (Fig. 6C), and classic resource competition theory predicts that the species surviving on the lowest resource abundance will outcompete others (65–67). Thus, the combined NSM steady-state dynamics and allometric timescales predict that larger

464 mammals have an intrinsic competitive advantage given a com-
465 mon resource, but does not offer a within-lineage mechanism by
466 which larger body sizes are selected for.

467 To examine whether the NSM could provide such a mecha-
468 nism, we begin by noting that a theoretical upper bound on
469 mammalian body size is given by $\epsilon_\sigma = 0$, where mammals
470 are entirely composed of metabolic reserves, and this occurs at
471 $M = 8.3 \times 10^8$, or 120× the mass of a male African elephant.

472 Next we examine to what extent a more realistic upper bound
473 to body mass may serve as an evolutionary attractor, thus pro-
474 viding a suitable within-lineage mechanism for Cope's rule. We
475 directly assess the susceptibility of an otherwise homogeneous
476 population to invasion by a mutated subset of the population
477 (denoted by ') where individuals have a modified proportion of
478 body fat $M' = M(1 + \chi)$ where $\chi \in [-f_0 M^{\gamma-1}, 0.05]$ (where
479 the lower bound of χ is the proportion of body mass that is
480 not composed of metabolic reserves and the upper bound main-
481 tains the organism's reproductive mass), thus altering the rates
482 of starvation $\sigma(M')$, recovery $\rho(M')$, and the maintenance of
483 both starving $\delta(M')$ and full consumers $\beta(M')$. Importantly,
484 ϵ_σ , which determines the point along the growth curve the de-
485 fines the state of starved foragers, is assumed to remain un-
486 changed for the invader population (see Supplemental Material
487 for detailed derivations of invader rates).

488 To assess the susceptibility of the resident population to
489 invasion, we determine which consumer has a lower steady-
490 state resource density for a given value of χ , again with the
491 expectation that populations able to survive on lower resource
492 densities have a competitive advantage (65). We find that for
493 $M \leq 1.73 \times 10^7$ g, having additional body fat ($\chi > 0$) results in
494 lower steady state resource density ($R^* < R'$), such that the
495 invader has an intrinsic competitive advantage over the resident
496 population. However, for $M > 1.73 \times 10^7$ g, leaner individuals
497 ($\chi < 0$) have lower resource steady state densities, switching
498 the advantage for higher values of M .

499 The observed switch in susceptibility as a function of χ at
500 $M_{\text{opt}} = 1.73 \times 10^7$ g thus serves as an attractor, such that the
501 NSM predicts organismal mass to increase if $M < M_{\text{opt}}$ and
502 decrease if $M > M_{\text{opt}}$. This value is close to but smaller than
503 the asymptotic upper bound for terrestrial mammal body size
504 predicted by the NSM, however it is remarkably close to in-
505 dependent estimates of the largest land mammals, the early
506 Oligocene *Indricotherium* at ca. 1.3×10^7 g and the late Miocene
507 *Deinotherium* at ca. 1.74×10^7 g (61). Additionally, our calcu-
508 lation of M_{opt} as a function of mass-dependent physiological rates
509 is similar to theoretical estimates of maximum body size (60),
510 and provides independent theoretical support for the observa-
511 tion of a 'maximum body size attractor' for North American
512 mammals outlined by Alroy (59). While the state of the envi-
513 ronment, as well as the competitive landscape, will determine
514 whether specific body sizes are selected for or against (62), we
515 propose that the dynamics of starvation and recovery described
516 in the NSM may provide a general within-lineage mechanism
517 for the evolution of larger body size among terrestrial mammals.
518

519 The energetics associated with somatic maintenance,
520 growth, and reproduction are important elements that influence
521 the dynamics of all populations (11). The NSM is a minimal
522 and general model that incorporates the dynamics of starvation
523 and recovery that are expected to occur in resource-limited en-
524 vironments. By incorporating allometric relations between the
525 rates in the NSM, we found: (i) different organismal masses
526 have distinct population dynamic regimes, (ii) allometrically-
527 determined rates of starvation and recovery appear to minimize
528 extinction risk, and (iii) the dynamic consequences of these rates
529 may introduce additional drivers and hard boundaries on the
530 evolution of maximum body size. We suggest that the NSM
531 offers a means by which the dynamic consequences of energetic

531 constraints can be assessed using macroscale interactions be-
532 tween and among species. Future efforts will involve exploring
533 the consequences of these dynamics in a spatially explicit frame-
534 work, thus incorporating elements such as movement costs and
535 spatial heterogeneity, which may elucidate additional tradeoffs
536 associated with the dynamics of starvation and recovery.

References

1. Martin TE (1987) Food as a Limit on Breeding Birds: A Life-History Perspective. *Annu. Rev. Ecol. Syst.* 18:453–487.
2. Kirk KL (1997) Life-History Responses to Variable Environments: Starvation and Reproduction in Planktonic Rotifers. *Ecology* 78:434–441.
3. Kempes CP, Dutkiewicz S, Follows MJ (2012) Growth, metabolic partitioning, and the size of microorganisms. *PNAS* 109:495–500.
4. Mangel M, Clark CW (1988) *Dynamic Modeling in Behavioral Ecology* (Princeton University Press, Princeton).
5. Mangel M (2014) Stochastic dynamic programming illuminates the link between environment, physiology, and evolution. *B. Math. Biol.* 77:857–877.
6. Yeakel JD, Dominy NJ, Koch PL, Mangel M (2014) Functional morphology, stable isotopes, and human evolution: a model of consilience. *Evolution* 68:190–203.
7. Morris DW (1987) Optimal Allocation of Parental Investment. *Oikos* 49:332.
8. Tveraa T, Fauchald P, Henaug C, Yoccoz NG (2003) An examination of a compensatory relationship between food limitation and predation in semi-domestic reindeer. *Oecologia* 137:370–376.
9. Daan S, Dijkstra C, Drent R, Meijer T (1988) *Food supply and the annual timing of avian reproduction*.
10. Jacot A, Valeu M, van Oers K, Kempenaers B (2009) Experimental nest site limitation affects reproductive strategies and parental investment in a hole-nesting passerine. *Animal Behaviour* 77:1075–1083.
11. Stearns SC (1989) Trade-Offs in Life-History Evolution. *Funct. Ecol.* 3:259.
12. Barboza P, Jorde D (2002) Intermittent fasting during winter and spring affects body composition and reproduction of a migratory duck. *J Comp Physiol B* 172:419–434.
13. Threlkeld ST (1976) Starvation and the size structure of zooplankton communities. *Freshwater Biol.* 6:489–496.
14. Weber TP, Ens BJ, Houston AI (1998) Optimal avian migration: A dynamic model of fuel stores and site use. *Evolutionary Ecology* 12:377–401.
15. Mduma SAR, Sinclair ARE, Hilborn R (1999) Food regulates the Serengeti wildebeest: a 40-year record. *J. Anim. Ecol.* 68:1101–1122.
16. Moore JW, Yeakel JD, Peard D, Lough J, Beere M (2014) Life-history diversity and its importance to population stability and persistence of a migratory fish: steelhead in two large North American watersheds. *J. Anim. Ecol.* 83:1035–1046.
17. Mead RA (1989) in *Carnivore Behavior, Ecology, and Evolution* (Springer US, Boston, MA), pp 437–464.
18. Sandell M (1990) The Evolution of Seasonal Delayed Implantation. *The Quarterly Review of Biology* 65:23–42.
19. Bulik CM, et al. (1999) Fertility and Reproduction in Women With Anorexia Nervosa. *J. Clin. Psychiatry* 60:130–135.
20. Trites AW, Donnelly CP (2003) The decline of Steller sea lions *Eumetopias jubatus* in Alaska: a review of the nutritional stress hypothesis. *Mammal Review* 33:3–28.

- 595 21. Glazier DS (2009) Metabolic level and size scaling of rates 661 45. Hou C, et al. (2008) Energy Uptake and Allocation During
596 of respiration and growth in unicellular organisms. *Funct. 662*
597 *Ecol.* 23:963–968.
598 22. Kooijman SALM (2000) *Dynamic Energy and Mass Bud-* 664 46. Bettencourt LMA, Lobo J, Helbing D, Kuhnert C, West
599 *gets in Biological Systems* (Cambridge). 665 GB (2007) Growth, innovation, scaling, and the pace of life
600 23. Sousa T, Domingos T, Poggiale JC, Kooijman SALM 666 47. Folland JP, Mc Cauley TM, Williams AG (2008) Allometric
601 (2010) Dynamic energy budget theory restores coherence 667 48. Calder III WA (1983) An allometric approach to population
602 in biology. *Philos. T. Roy. Soc. B* 365:3413–3428. 668 cycles of mammals. *J. Theor. Biol.* 100:275–282.
603 24. Diekmann O, Metz JAJ (2010) How to lift a model for in- 669 49. Peterson RO, Page RE, Dodge KM (1984) Wolves, Moose,
604 dividual behaviour to the population level? *Philos. T. Roy. 670*
605 *Soc. B* 365:3523–3530.
606 25. Murdoch WW, Briggs CJ, Nisbet RM (2003) *Consumer- 671*
607 *resource Dynamics*, Monographs in population biology 672 50. Krukonis G, Schaffer WM (1991) Population cycles in mam-
608 (Princeton University Press). 673
609 26. Benichou O, Redner S (2014) Depletion-Controlled Starva- 674 51. Hendriks AJ, Mulder C (2012) Delayed logistic and Rosen-
610 tion of a Diffusing Forager. *arXiv*. 675 zweig–MacArthur models with allometric parameter setting
611 27. Bénichou O, Chupeau M, Redner S (2016) Role of Deple- 676 estimate population cycles at lower trophic levels well. *Eco-
612 tion on the Dynamics of a Diffusing Forager. 677 logical Complexity* 9:43–54.
613 28. Chupeau M, Bénichou O, Redner S (2016) Universality 678 52. Kendall BE, et al. (1999) Why do populations cycle? A syn-
614 classes of foraging with resource renewal. *Phys. Rev. E* 679
615 93:032403.
616 29. Persson L, Leonardsson K, De Roos AM, Gyllenberg M, 680 53. Höglstedt G, Seldal T, Breistol A (2005) Period length in
617 Christensen B (1998) Ontogenetic Scaling of Foraging Rates 681 cyclic animal populations. *Ecology* 86:373–378.
618 and the Dynamics of a Size-Structured Consumer-Resource 682 54. Kendall, Prendergast, Bjornstad (1998) The macroecology
619 Model. *Theoretical Population Biology* 54:270–293.
620 30. Murray JD (2011) *Mathematical Biology: I. An Introduct-* 683 55. Brown J, Marquet P, Taper M (1993) Evolution of body
621 *ion, Interdisciplinary Applied Mathematics* (Springer New 684 size: consequences of an energetic definition of fitness. *Am.*
622 York) Vol. 110. 685 *Nat.* 142:573–584.
623 31. Strogatz SH (2008) *Nonlinear Dynamics and Chaos*, With 686 56. West GB, Brown JH, Enquist BJ (1997) A General Model
624 Applications to Physics, Biology, Chemistry, and Engineer- 687 for the Origin of Allometric Scaling Laws in Biology. *Sci-
625 ing* (Westview Press). 688
626 32. Guckenheimer J, Holmes P (1983) *Nonlinear oscilla- 689 57. West GB, Woodruff WH, Brown JH (2002) Allometric scal-
627 tions, dynamical systems, and bifurcations of vector fields* 690 691 ing of metabolic rate from molecules and mitochondria to
628 (Springer, New York). 692 cells and mammals. *Proc. Natl. Acad. Sci. USA* 99:2473–
629 33. Gross T, Feudel U (2004) Analytical search for bifurcation 693 2478.
630 surfaces in parameter space. *Physica D* 195:292–302. 694
631 34. Hastings A (2001) Transient dynamics and persistence of 695 58. Millar J, Hickling G (1990) Fasting Endurance and the
632 ecological systems. *Ecol. Lett.* 4:215–220. 696
633 35. Neubert M, Caswell H (1997) Alternatives to resilience for 697 59. Alroy J (1998) Cope’s rule and the dynamics of body
634 measuring the responses of ecological systems to perturba- 698 699 mass evolution in North American fossil mammals. *Science*
635 tions. *Ecology* 78:653–665. 700 280:731.
636 36. Caswell H, Neubert MG (2005) Reactivity and transient 701 60. Clauzel A, Redner S (2009) Evolutionary Model of Species
637 dynamics of discrete-time ecological systems. *Journal of 702 Body Mass Diversification. Phys. Rev. Lett.* 102:038103.
638 Difference Equations and Applications 11:295–310. 703
639 37. Neubert M, Caswell H (2009) Detecting reactivity. *Ecology*. 704 61. Smith FA, et al. (2010) The Evolution of Maximum Body
640 38. Yodzis P, Innes S (1992) Body Size and Consumer-Resource 705 705 Size of Terrestrial Mammals. *Science* 330:1216–1219.
641 Dynamics. *Am. Nat.* 139:1151–1175. 706
642 39. Brown J, Gillooly J, Allen A, Savage V, West G (2004) To- 707 62. Saarinen JJ, et al. (2014) Patterns of maximum body size
643 ward a metabolic theory of ecology. *Ecology* 85:1771–1789. 708 708 evolution in Cenozoic land mammals: eco-evolutionary pro-
644 40. West GB, Woodruff WH, Brown JH (2002) Allometric scal- 709 709 cesses and abiotic forcing. *Proc Biol Sci* 281:20132049–
645 ing of metabolic rate from molecules and mitochondria to 710 20132049.
646 cells and mammals. *Proc. Natl. Acad. Sci. USA* 99 Suppl 711 63. Allen AP, Brown JH, Gillooly JF (2002) Global Biodiver-
647 1:2473–2478. 712 712 sity, Biochemical Kinetics, and the Energetic-Equivalence
648 41. DeLong JP, Okie JG, Moses ME, Sibly RM, Brown JH 713 Rule. *Science* 297:1545–1548.
649 (2010) Shifts in metabolic scaling, production, and effi- 714 64. Enquist BJ, Brown JH, West GB (1998) Allometric scal-
650 ciency across major evolutionary transitions of life. *PNAS* 715 715 ing of plant energetics and population density : Abstract :
651 107:12941–12945. 716 716 Nature. *Nature* 395:163–165.
652 42. West GB, Brown JH, Enquist BJ (2001) A general model 717 65. Tilman D (1981) Tests of Resource Competition Theory Us-
653 for ontogenetic growth. *Nature* 413:628–631. 718 719 ing Four Species of Lake Michigan Algae. *Ecology* 62:802–
654 43. Moses ME, et al. (2008) Revisiting a Model of Ontogenetic 720 720 815.
655 Growth: Estimating Model Parameters from Theory and 721 66. Dutkiewicz S, Follows MJ, Bragg JG (2009) Modeling the
656 Data. <http://dx.doi.org.proxy.lib.sfu.ca/10.1086/679735> 722 723 coupling of ocean ecology and biogeochemistry. *Global Bio-
657 171:632–645. 724 724 geochem. Cycles* 23:1–15.
658 44. Gillooly JF, Charnov EL, West GB, Savage VM, Brown JH 725 67. Barton AD, Dutkiewicz S, Flierl G, Bragg J, Follows MJ
659 (2002) Effects of size and temperature on developmental 726 726 (2010) Patterns of Diversity in Marine Phytoplankton. *Sci-
660 time. *Nature* 417:70–73. 727 727 ence* 327:1509–1511.

⁷²⁷ **ACKNOWLEDGMENTS.** We thank Luis Bettencourt, Jean Philippe Gibert, ⁷³¹ was supported by an Omidyar Postdoctoral Fellowship at the Santa Fe Institute.
⁷²⁸ Eric Libby, and Seth Newsome for helpful discussions and comments on the ⁷³² S.R. was supported by grants DMR-1608211 and 1623243 from the National
⁷²⁹ manuscript. J.D.Y. was supported by startup funds at the University of California, ⁷³³ Science Foundation, and by the John Templeton Foundation, all at the Santa Fe
⁷³⁰ Merced, and an Omidyar Postdoctoral Fellowship at the Santa Fe Institute. C.P.K. ⁷³⁴ Institute.

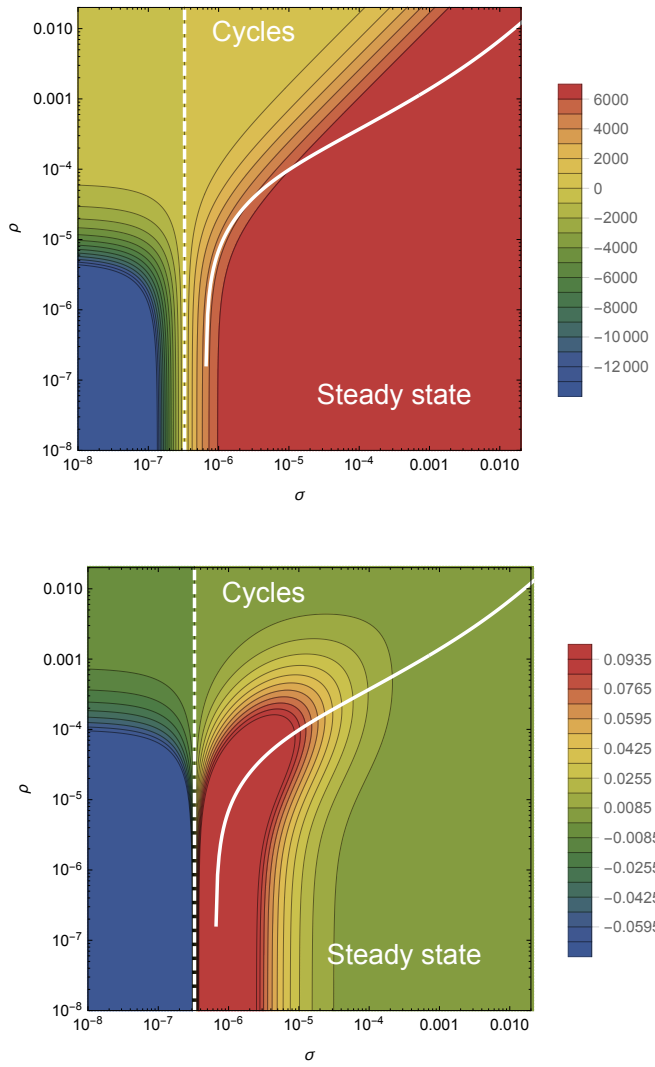


Fig. 1: The transcritical (dashed) and Hopf bifurcation (solid) as a function of the starvation rate σ and recovery rate ρ for a 100g consumer. These bifurcation conditions separate parameter space into infeasible, cyclic, and steady state dynamic regimes. The color gradient shows the steady state densities for (A) the resource R^* and the (B) energetically replete consumers F^* , (warmer colors denote higher densities). Steady state densities for the energetically deficient consumers H^* (not shown) scale with those for F^* .

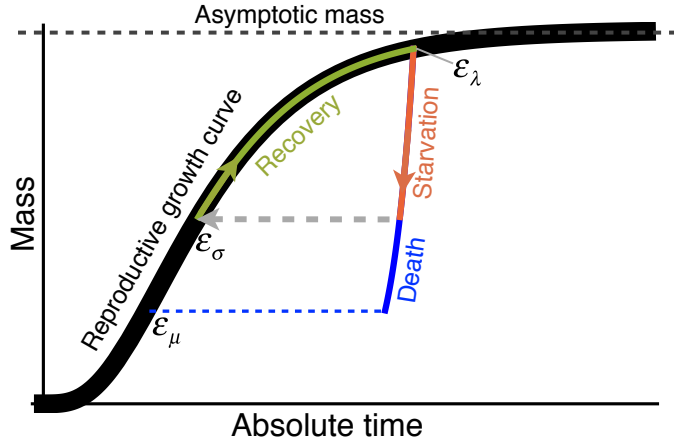


Fig. 2: The growth trajectory over absolute time of an individual organism as a function of body mass. Initial growth follows the black trajectory to an energetically replete reproductive adult mass $m = \epsilon_\lambda M$ which we assume is 95% asymptotic mass M . Starvation follows the red trajectory to $m = \epsilon_\sigma \epsilon_\lambda M$, and recovery follows the green growth trajectory to the replete adult mass. Alternatively, death from starvation follows the blue trajectory to $m = \epsilon_\mu \epsilon_\lambda M$.

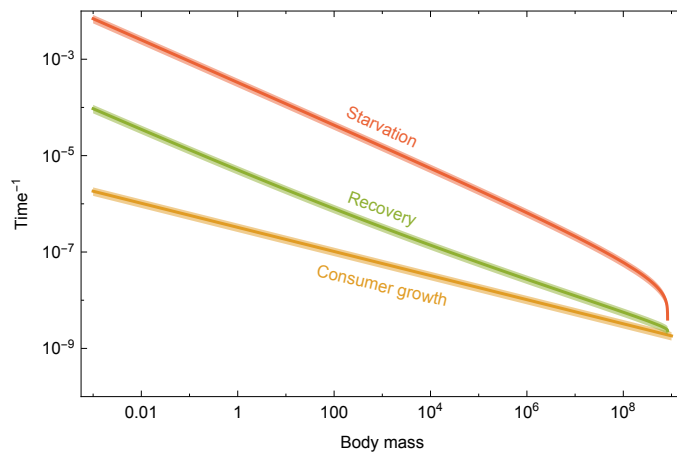


Fig. 3: Allometrically constrained starvation rate σ (red) and recovery rate ρ (green) relative to the reproductive rate λ (orange) as a function of body mass. The rate of starvation is greater than the rate of reproduction for all realized terrestrial endotherm body sizes. Mean values $\pm 20\%$ variation are shown by the shaded region for each rate.

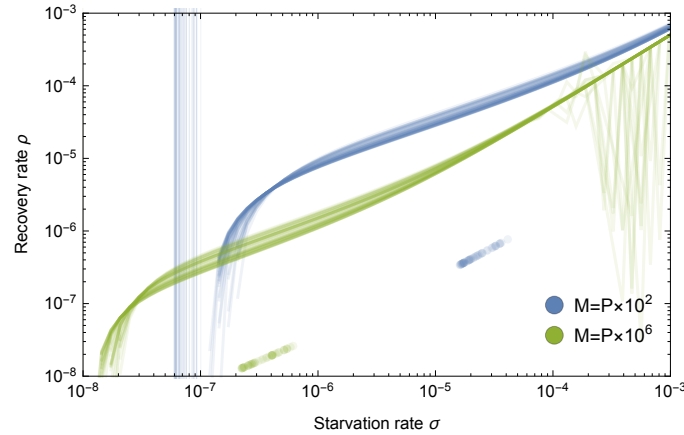


Fig. 4: Transcritical (vertical lines) and Hopf bifurcations (curves) for allometrically determined starvation σ and recovery ρ rates as a function of different mammalian body sizes: $M = P \times 10^2\text{g}$ (blue) and $M = P \times 10^6\text{g}$ (green), where P is a random uniform variable in $[1, 9]$. Points denote realized values of σ and ρ given the drawn values for M .

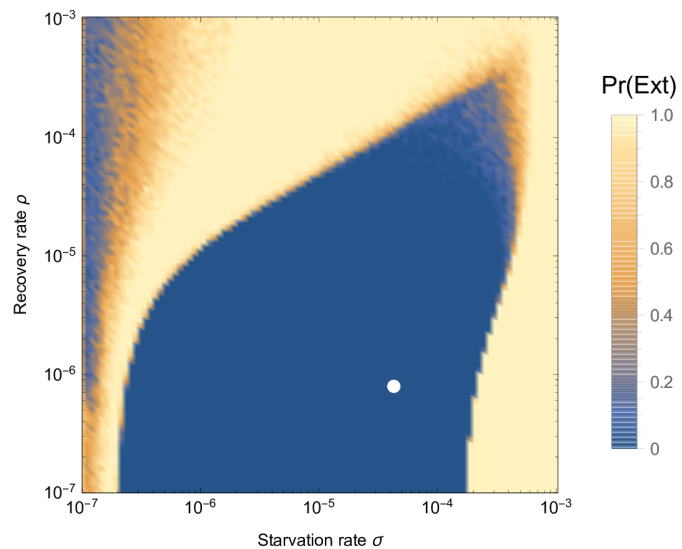


Fig. 5: Probability of extinction for a 100g consumer as a function of the starvation rate σ and recovery rate ρ , where the initial density is given as $A(F^*, H^*, R^*)$, with A being a random uniform variable in $[0, 2]$. Extinction is defined as the population trajectory falling below $0.1 \times$ the allometrically constrained steady state. The white point denotes the allometrically constrained starvation and recovery rate.

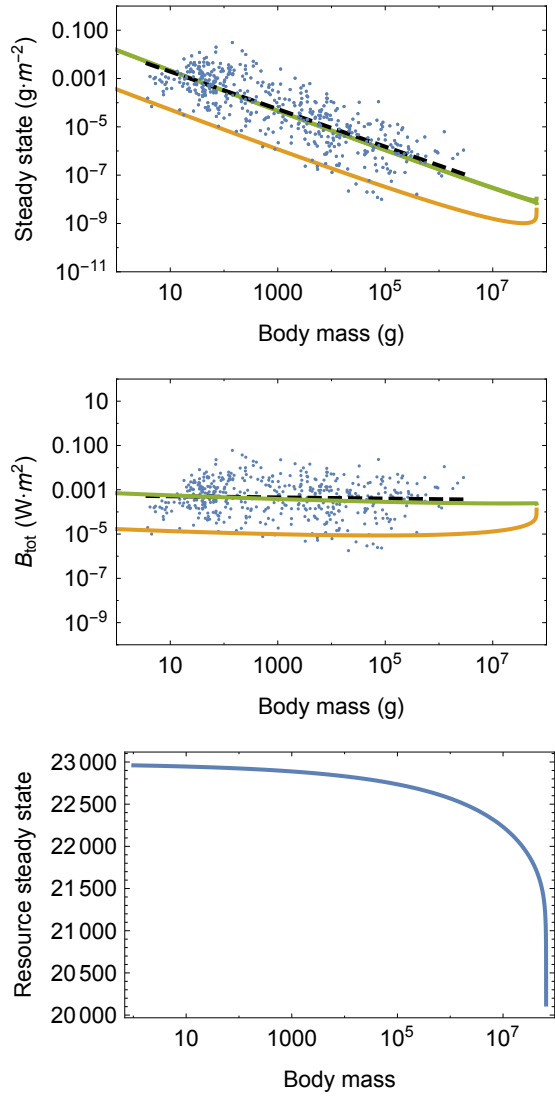


Fig. 6: (A) Consumer steady states F^* (green) and H^* (orange) as a function of body mass. (B) Total energetic use B_{tot} of consumer populations at the steady state as a function of body mass. (C) Resource steady state R^* as a function of consumer body mass.

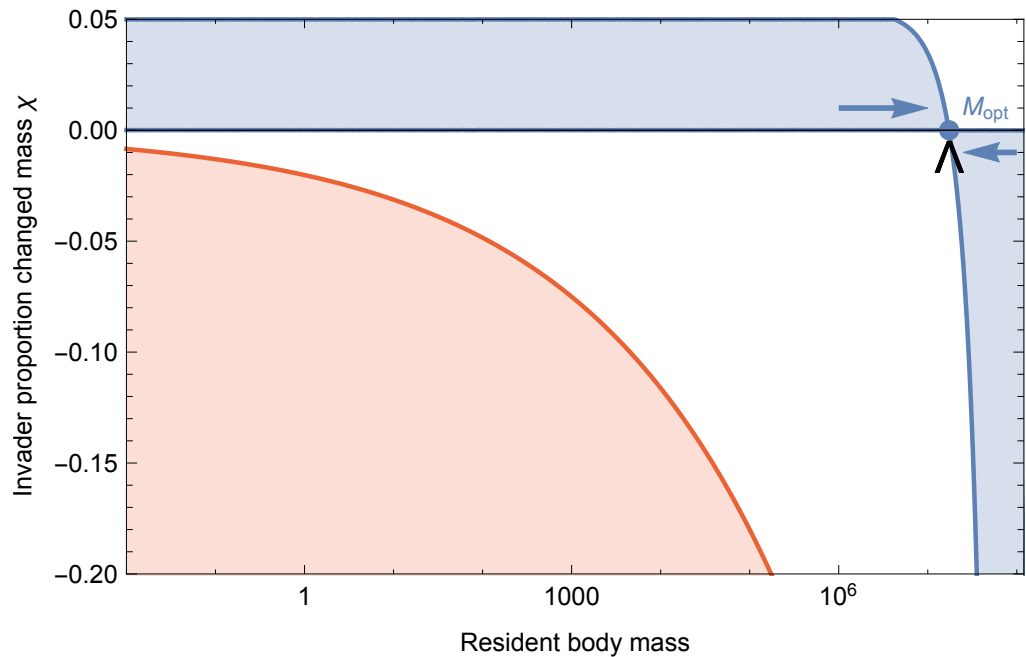


Fig. 7: Invasion feasibility for organisms with a proportional change in mass χ against a population with a resident body mass M . The blue region denotes proportions of modified mass χ resulting in successful invasion. The red region denotes values of χ that result in a mass that is below the starvation threshold and is thus infeasible. Arrows point to the predicted optimal mass $M_{\text{opt}} = 1.73 \times 10^7$, which serves as an evolutionary attractor for body mass. The black wedge points to the largest body mass known for terrestrial mammals at $7.4 \times 10^7 \text{ g}$ (61).